Extreme Ultraviolet Observations from the Voyager 2 Encounter with Saturn

B. R. Sandel; D. E. Shemansky; A. L. Broadfoot; J. B. Holberg; G. R. Smith; J. C. McConnell; D. F. Strobel; S. K. Atreya; T. M. Donahue; H. W. Moos; D. M. Hunten; R. B. Pomphrey; S. Linick

Science, New Series, Vol. 215, No. 4532 (Jan. 29, 1982), 548-553.

Stable URL:
http://links.jstor.org/sici?sici=0036-8075%2819820129%293%3A215%3A4532%3C548%3AEUOFTV%3E2.0.CO%3B2-M

Science is currently published by American Association for the Advancement of Science.

---

geneous, nonscattering slab that radiates as a blackbody. The observed thermal emission as a function of wave number, I_ν, will then be related to the blackbody emission of the material, $B_\nu(T_{ring})$, by

$$I_\nu = (1 - e^{-\tau_{ring}/\cos\theta}) B_\nu(T_{ring})$$

where T_{ring} and τ_{ring} are the blackbody temperature and normal infrared optical depth of the ring material and θ is the emission angle measured from the ring plane normal.

From averages of pairs of spectra in the ring scan, intensities at 200 and 400 cm^{-1} were used to derive normal infrared optical depths and ring temperatures (Fig. 8, b and c). If the system is optically thick the optical depth is poorly determined because of sensitivity to noise, as is evident for the B ring (Fig. 8b). The results are summarized in Table 1. The results for the C ring are in agreement with those from Pioneer (*15*) and are identical to those derived from Voyager 1 data by applying the above model to observed variations of infrared intensity with emission angle (*3*). No similar calculations were made for the A and B rings with Voyager 1 data. The normal optical depths of the A and C rings and of the Cassini division are in agreement with values at similar spatial resolution at shorter wavelengths (*11, 15, 16*). Discrepancies may exist with longer wavelength observations (*15, 17*). The sensitivity of the simple model to noise for an optically thick system and the neglect of phase angle corrections and of mutual shadowing among ring particles make detailed quantitative comparison of these results with other data premature.

R. HANEL
B. CONRATH
F. M. FLASAR
V. KUNDE
W. MAGUIRE
J. PEARL
J. PIRRAGLIA
R. SAMUELSON
NASA Goddard Space Flight Center, Greenbelt, Maryland 20771
D. CRUIKSHANK
University of Hawaii, Honolulu 96822
D. GAUTIER
Paris Observatory, Meudon, France
P. GIERASCH
Cornell University, Ithaca, New York 14853
L. HORN
Jet Propulsion Laboratory, Pasadena, California 91109
C. PONNAMPERUMA
University of Maryland, College Park 20742

References and Notes

1. R. A. Hanel *et al.*, *Science* **206**, 952 (1979).
2. R. A. Hanel *et al.*, *ibid.* **204**, 972 (1979); J. Pearl, R. Hanel, V. Kunde, W. Maguire, K. Fox, S. Gupta, C. Ponnamperuma, F. Raulin, *Nature (London)* **280**, 755 (1979); R. A. Hanel, B. J. Conrath, L. W. Herath, V. G. Kunde, J. A. Pirraglia, *J. Geophys. Res.* **86**, A10, 8705 (1981); D. Gautier, B. Conrath, M. Flasar, R. Hanel, V. Kunde, *ibid.*, p. 8713; B. J. Conrath, F. M. Flasar, J. A. Pirraglia, P. J. Gierasch, G. E. Hunt, *ibid.*, p. 8769; F. M. Flasar, B. J. Conrath, J. A. Pirraglia, P. C. Clark, R. G. French, P. J. Gierasch, *ibid.*, p. 8759; G. Hunt, B. Conrath, J. Pirraglia, *ibid.*, p. 8777; A. Marten *et al.*, *Icarus* **46** (1981).
3. R. A. Hanel *et al.*, *Science* **212**, 192 (1981).
4. J. A. Pirraglia, B. J. Conrath, M. D. Allison, P. J. Gierasch, *Nature (London)* **292**, 677 (1981).
5. F. M. Flasar, R. E. Samuelson, B. J. Conrath, *ibid.*, p. 693.
6. W. C. Maguire, R. A. Hanel, D. E. Jennings, V. G. Kunde, R. E. Samuelson, *ibid.*, p. 683; V. G. Kunde, A. C. Aikin, R. A. Hanel, D. E. Jennings, W. C. Maguire, R. E. Samuelson, *ibid.*, p. 686; R. E. Samuelson, R. A. Hanel, V. G. Kunde, W. C. Maguire, *ibid.*, p. 688.
7. R. Hanel, D. Crosby, L. Herath, D. Vanous, D. Collins, H. Creswick, C. Harris, M. Rhodes, *Appl. Opt.* **19**, 1391 (1980).
8. B. J. Conrath and D. Gautier, in *Remote Sensing of Atmospheres and Oceans*, A. Deepak, Ed. (Academic Press, New York, 1980), p. 611.
9. P. J. Gierasch and R. M. Goody, *J. Atmos. Sci.* **26**, 979 (1969).
10. B. A. Smith *et al.*, *Science* **215**, 504 (1982).
11. B. A. Smith *et al.*, *ibid.* **212**, 163 (1981).
12. D. P. Cruikshank and T. J. Jones, *Icarus* **31**, 427 (1977).
13. J. M. Saari, R. W. Shorthill, D. F. Winter, *Moon* **5**, 179 (1972).
14. D. Morrison, in *Planetary Satellites*, J. A. Burns, Ed. (Univ. of Arizona Press, Tucson, 1977), p. 269.
15. L. Froidevaux and A. P. Ingersoll, *J. Geophys. Res.* **85**, 5929 (1980).
16. L. W. Esposito, J. P. Dilley, J. W. Fountain, *ibid.*, p. 5948; B. R. Sandel *et al.*, *Science* **215**, 548 (1982).
17. G. L. Tyler, V. R. Eshleman, J. D. Anderson, G. S. Levy, G. G. Lindal, G. E. Wood, T. A. Croft, *ibid.* **212**, 201 (1981).
18. We thank L. Mayo, J. Frost, J. Tingley, and J. Hornstein for their support in data processing and programming.

10 November 1981

Extreme Ultraviolet Observations from the Voyager 2 Encounter with Saturn

Abstract. *Combined analysis of helium (584 angstroms) airglow and the atmospheric occultations of the star δ Scorpii imply a vertical mixing parameter in Saturn's upper atmosphere of* K *(eddy diffusion coefficient) ~ 8 × 10⁷ square centimeters per second, an order of magnitude more vigorous than mixing in Jupiter's upper atmosphere. Atmospheric H_2 band absorption of starlight yields a preliminary temperature of 400 K in the exosphere and a temperature near the homopause of ~ 200 K. The energy source for the mid-latitude H_2 band emission still remains a puzzle. Certain auroral emissions can be fully explained in terms of electron impact on H_2, and auroral morphology suggests a link between the aurora and the Saturn kilometric radiation. Absolute optical depths have been determined for the entire C ring and parts of the A and B rings. A new eccentric ringlet has been detected in the C ring. The extreme ultraviolet reflectance of the rings is fairly uniform at 3.5 to 5 percent. Collisions may control the distribution of H in Titan's H torus, which has a total vertical extent of ~ 14 Saturn radii normal to the orbit plane.*

Saturn's atmosphere. The H, H_2, and He of Saturn's upper atmosphere emit characteristic radiation in the extreme ultraviolet (EUV) wavelengths. Although resonance scattering of the strong solar lines at H Lyman α and He 584 Å accounts for much of the equatorial and mid-latitude emission at those wavelengths, mid-latitude emissions originating from electron-excited H and H_2 were also observed.

The brightness of the He 584 Å line increased from 2.2 ± 0.3 rayleigh (R) during the Voyager 1 encounter (*1*) to 4.2 ± 0.5 R during the Voyager 2 encounter, indicating that important changes have occurred in the upper atmosphere (*2*). Models of the He 584 Å dayglow (*3*) require either a decrease of the temperature (*T*) in the scattering region or an increase in the eddy diffusion coefficient (*K*) (*4*) to account for the observed change. The H Lyα brightness should be strongly anticorrelated with the He 584 Å brightness (*3*), whereas only a slight decrease from 3.3 kR (Voyager 1) to 3.0 kR (Voyager 2) was observed.

In principle it is possible to derive a value of *K* from the H Lyα brightness (*5*) and remove the *T-K* ambiguity, but in practice this procedure leads to uncertain results because H Lyα can be excited by mechanisms other than resonance scattering of the solar line, and H can be supplied by processes other than dissociation of molecules by solar radiation (*6*). Elsewhere (*7*) we combine information obtained from a stellar occultation with the He model to derive a *T*, *K* pair consistent with both sets of data. The values are $K \sim 8 \times 10^7$ cm^2 sec^{-1} and $T = 170$ K near the homopause. The large H Lyα brightness of the planet can probably be reconciled with the large value of *K*, given the possibility of additional excitation mechanisms and additional sources of H. The equatorial and mid-latitude H_2 band intensity was the same at both encounters.

Measurements of H_2 band emissions from Saturn's mid-latitudes have empha-

0036-8075/82/0129-0548$01.00/0

sized a deficiency in our understanding of the excitation mechanism for these bands (*1, 8*) at Saturn and Jupiter. Illumination of the atmosphere by sunlight is observed to be a necessary condition for the production of the H_2 band emissions, which must be electron-excited. Yet insufficient energy is available in the solar flux alone, suggesting the existence of an additional source of energy. Voyager 2 measurements show that the H_2 band intensity in the shadow of the rings is less than 15 percent of its value just north of the shadow. This fact, and the sharp edge of the ring shadow, are further evidence against excitation by precipitating magnetospheric particles. Comparison of the H_2 band intensitites at the bright and dark limbs places an upper limit of 0.3 hour on the $(1/e)$ time constant for the decay of any nonsolar excitation process.

Occultations of the sun and of the bright UV star δ Scorpii (δ Sco) by the atmosphere of Saturn were observed by the ultraviolet spectrometer (UVS). By means of this measurement the wavelength-dependent absorption of light by the atmosphere is used to infer the composition and structure of the atmosphere. Absorption near 1200 Å, where H_2 absorption is negligible, shows a scale height of 12 ± 2 km just above the homopause, implying a temperature of 200 ± 30 K if CH_4 is the absorber, consistent with the temperature of 170 K mentioned above. This temperature applies near an optical depth of 1, ~ 1150 km above the 1-bar pressure level. At higher levels, the temperature is higher. Figure 1 shows a light curve from the occultation compared with the curve expected from two models, both including H_2 and CH_4 absorption and having $T = 200$ K at the homopause but with different exospheric temperatures. For distant stars such as δ Sco the interstellar medium completely absorbs all stellar flux shortward of 912 Å, where H and H_2 absorb into the continuum. Atmospheric absorption of the starlight longward of 912 Å is therefore due to the Lyman and Werner bands of H_2. Absorption in these bands has been included in the model curves. The 400 K curve fits the data in the 1600-km altitude range significantly better than the 800 K curve, indicating a provisional exospheric temperature lower than reported earlier (*1*) from the solar occultation, which was probably biased toward larger scale heights by the finite size of the sun. Detailed modeling of the solar occultations observed by Voyager 1 and Voyager 2 is expected to resolve the discrepancy in favor of the lower value.

Auroral excitation spectrum of H_2. The auroral spectrum in Fig. 2 is of particular interest because it shows an $e + H_2$ spectrum almost uncontaminated by other excitation components. The model calculation [described in detail in (*9*) and shown in Fig. 2] contains only the direct products of the $e + H_2$ process. The observation is important for the following reasons. (i) It is now clear that we have an accurate model of the $e + H_2$ excitation process. The result is therefore a benchmark for the analysis of other more complex auroral spectral structures (*8*). The consistency with pure $e + H_2$ excitation includes the intensity ratio of H Lyα to H_2 band emission as measured in the laboratory. (ii) The laboratory measurements of the relative cross sections of the H_2 band system are now in good agreement with theoretical calculations (*9, 10*), thus establishing the accuracy of the relative instrument calibration in the 850 to 1700 Å region. The observations of other emissions can now be accurately interpreted in terms of composition, vibrational excitation, and fluorescence and reflection of solar radiation, whereas such interpretations could not be made before.

The model calculation includes all of the measurable EUV transitions in $e + H_2$ excitation, $(B\ ^1\Sigma_u^+ - X\ ^1\Sigma_g^+)$ discrete and continuum transitions, $(E, F\ ^1\Sigma_g^+ - B\ ^1\Sigma_u^+)$, $(B'\ ^1\Sigma_u^+ - X\ ^1\Sigma_g^+)$, $(B''\ ^1\Sigma_u^+ - X\ ^1\Sigma_g^+)$, $(C\ ^1\Pi_u - X\ ^1\Sigma_g^+)$, $(D$

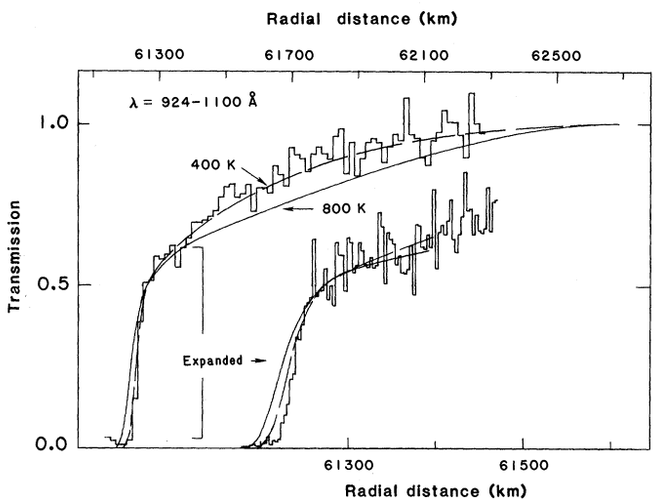

Fig. 1 (left). Transmission (924 to 1100 Å) plotted against altitude measured during the δ Sco exit occultation. Above 61,400 km the starlight is attenuated by absorption in the H_2 bands. The rapid increase in absorption near 61,300 km (expanded scale) is due to a hydrocarbon, probably CH_4. The model curves show the transmission expected for an atmosphere consisting of CH_4 and H_2 with a mixing ratio of 0.08 and a temperature of 200 K near the homopause and the indicated exospheric temperatures of 400 K (dashed line) and 800 K (solid line). Fig. 2 (right). North polar aurora on Saturn. The position of the UVS slit in relation to the auroral zone is shown in the inset. The light line shows the auroral spectrum from the UVS polar drift sequence near 0717 SCET on 25 August. The heavy line shows the model calculation of $e + H_2$ excitation transmitted through a foreground gas column of 10^{20} cm^{-2} of H_2 and 8×10^{15} cm^{-2} of CH_4 (*9*).

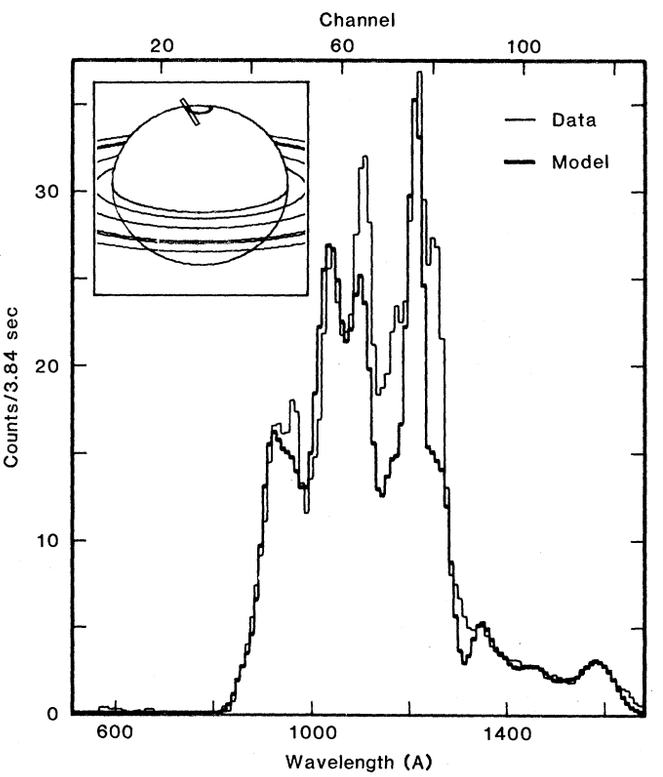

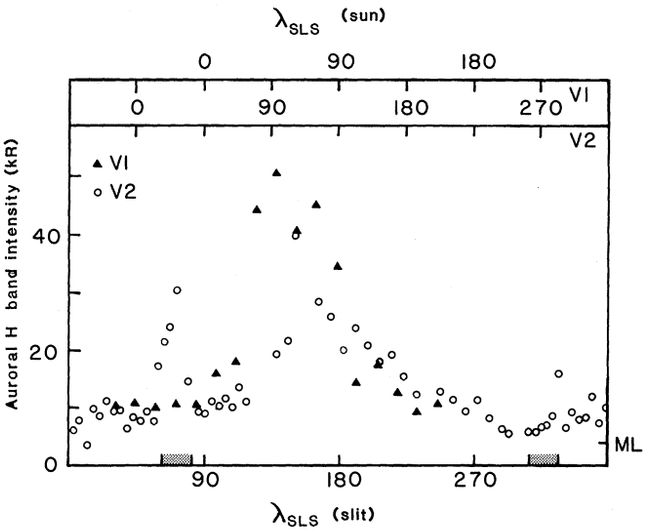

Fig. 3. Auroral brightness inferred from the 1105-Å H_2 band feature plotted against the longitude of the point at which the UVS slit crosses 80°N. Both Voyager 1 and Voyager 2 measured brightenings near $\lambda_{SLS} = 135°$. In both measurements, the brightenings occurred when the sun was near $\lambda_{SLS} \sim 100°$, suggesting that they may be related to the Saturn kilometric radiation. The longitudes indicated by shading were sampled by Voyager 2 one planet rotation period prior to the main map; the Voyager 1 observation was continuous in time. The tick marked *ML* shows the equivalent auroral brightness corresponding to the count rate that would result if the slit were filled by H_2 band emission of the brightness of Saturn's mid-latitudes.

$^1\Pi_u - X\ ^1\Sigma_g^+$), ($D'\ ^1\Pi_u - X\ ^1\Sigma_g^+$), and H I ($1s - 2p$). The H_2 B and C states are the first members of the σ and π Rydberg series in H_2 (*11*). The higher members of the series to $n = 4$ have now been found to make a measurable contribution to the emission spectrum (*10*), in accord with theoretical oscillator strengths for the higher series members (*9*).

The spectrum in Fig. 2 was obtained near 80°N latitude. Using the location of the auroral zone determined from Voyager 1 (*1*) we estimated the slit to be approximately one-third filled with auroral emission. This implies an apparent brightness of 100 kR in the H_2 (C–X) and (B–X) bands integrated along the line-of-sight tangent to the limb. This intensity is seven to ten times brighter than other observations in both encounters. Large intensity variations are expected in earth-like auroral events and this single Voyager 2 observation does not imply that the mean intensity of the north polar aurora has increased. The $e + H_2$ model requires an H_2 column abundance of 10^{20} cm^{-2} and a small column abundance of CH_4, 8×10^{15} cm^{-2}, in order to fit the observation shown in Fig. 2. The result implies penetration of the exciting particles to the density level of $[H_2] \sim 2 \times 10^{11}$ cm^{-3}. If the exciting primary particles are electrons their primary energy must be ~ 10 keV, the average primary energy of earth auroral electrons. This particularly bright spectrum (Fig. 2) originates much deeper in the atmosphere than most of the weaker Saturn auroral spectra. The weaker spectra appear to originate near the exobase and require no CH_4 absorption in the modeling process.

Auroral morphology. Voyager 2 has generally confirmed the picture of Saturn's auroras inferred from Voyager 1 observations (*1, 12*). During the Voyager 2 north-south map (NSM) sequence the UVS recorded the boreal aurora at all longitudes and near 9:00 local time with a brightness comparable to that measured by Voyager 1. Maps of the north polar region at higher spatial resolution are consistent with confinement of the boreal aurora within 12° of the pole, as is the case in the south. Strong variations in the brightness of the boreal aurora were recorded during the Voyager 2 NSM sequence. These variations were similar in many respects to those already reported on the basis of Voyager 1 data.

Auroral brightness variations measured during the two preencounter NSM sequences are compared in Fig. 3. The Voyager 1 brightness has been taken from Sandel and Broadfoot (*12*) and their assumptions have been used to infer the surface brightness measured by Voyager 2. For both encounters the slit extended over the auroral oval and mid-latitudes of the planet. The contribution to the signal from mid-latitude H_2 band emission has not been subtracted, but the level is shown. Although the signal near $\lambda_{SLS} = 300°$ falls close to the mid-latitude level, detailed examination of the data show that polar brightening is present in all longitudes. Both observations are consistent with a zonal brightening at $50° < \lambda_{SLS} < 180°$. In addition, both are consistent with a planetwide temporal brightening of the aurora when the longitude of the noon meridian is near 50° to 100°. Analysis of other auroral observations taken at other local times may remove this ambiguity. In any case, the remarkable similarity between the two observations argues that the structure is a real feature of Saturn's aurora, and not simply due to random brightness fluctuations. However, temporal variations are also present.

Sequence design requirements prevented continuous longitude coverage of Saturn during the NSM; instead the two longitude ranges shown shaded in Fig. 3 were observed one Saturn rotation period prior to the main map. Thus there are five instances where similar longitude ranges were sampled at an interval of 10 hours 40 minutes. The data have been taken out of their time sequence and ordered by λ_{SLS} in Fig. 3. The discontinuities in signal level before and after the "fill-in" block near $\lambda_{SLS} = 75°$ indicate purely temporal fluctuations, since they represent measurements made at different times but at the same local time and nearly the same λ_{SLS}. However, the discontinuity is consistent with a zonal motion of a brighter region; that is, the temporal variation may be simply small zonal excursions of a bright region about a mean longitude.

This suggests that the brightness variations are related to the Saturn kilometric radiation (SKR). Kaiser *et al.* (*13*) have shown that the source of the SKR may lie near 80°N latitude and in the λ_{SLS} range of 0° to 120°. The source would thus lie at the latitude of the aurora. In this framework, a planetwide temporal brightening of the aurora could result from a general increase in particle precipitation triggered by passage of a particular meridian through local noon. Perhaps a more likely possibility is a zonal asymmetry in auroral brightness due to increased precipitation in a region of anomalous magnetic field. An interaction between this field anomaly and a feature of the dayside magnetosphere could then trigger the SKR (*13*). In either case, it seems likely that the brightness variations in the aurora and the SKR are closely linked, as originally suggested by Sandel and Broadfoot (*12*). The brightening recorded near $\lambda_{SLS} = 70°$ is well within the SKR source region as well, and hence is consistent with the picture presented here.

Ring occultation. A double occultation of the star δ Sco (HD143275, B0.5 IV, V = 2.32) by the rings of Saturn was observed by the UVS. The first occultation preceded the entrance of δ Sco into Saturn's dayside atmosphere and covered the portion of the C ring between 1.43 and 1.29 R_S. The second covered the exit of δ Sco from the top of the atmosphere through the F ring, all within

the shadow of the planet. The apparent radial velocity of the star through the rings was ~ 10 km sec^{-1}, giving a resolution of about 3 km. The line of sight to δ Sco intercepted the ring plane at an angle of 28.71°, so that observed optical depths are multiplied by the sine of this angle to obtain normal optical depths (τ_n). The fact that there is no stellar signal shortward of 912 Å allows us to accurately estimate our dark count level. This together with a strong signal (900 counts per 0.32-second spectrum) makes possible a wide dynamic range in the determination of absolute optical depths.

Spectra averaged over portions of the A, B, and C rings as well as the Cassini division exhibited only neutral (spectrally flat) absorption between 912 and 1700 Å. Because of the short absorption path length, this result imposes little significant constraint on the density of molecular species. However, it does indicate the probable lack of a significant population of wavelength (0.1 μm) sized particles.

The C ring consists of a large number of easily recognizable ringlets of varying width and optical depth embedded in a generally unbroken ring of lower optical depth. The underlying optical depth of the C ring ranges from very low ($\tau_n < 0.05$) for its inner portions to $\tau_n \sim 0.15$ in its outer portions. The optical depths we have measured between ringlets are comparable to those found by Esposito *et al.* (*14*) from the Pioneer 11 results. In Fig. 4 we show preliminary normal optical depths plotted against planetocentric ring radius for the C ring. These results, which have been averaged over 50 km, show a great deal of structure because of the embedded ringlets of higher optical depth.

A comparison of the two occultations over the same portion of the C ring shows that the C ring is remarkably symmetrical with respect to the center of Saturn. This portion of the C ring (1.43 to 1.29 R_S) contains six prominent ringlets. Five of these features show an almost identical appearance on both sides of the planet. Radii (*15*) of these five features agree to within 7 km as determined from the preliminary spacecraft trajectory. In Fig. 5 we show the normal optical depths observed for three of these features on both the occultations. The innermost of these ringlets, located at 77,865 km, consists of a pair of very narrow ringlets of large optical depth ($\tau_n > 1$) separated by 3 to 6 km. On the dayside these ringlets have a total width of ~ 30 km, whereas on the nightside they are 19 km in total width and displaced 32 km closer to the planet. Figure 5 shows the eccentric ringlet as it appears in both the ingress and egress occultations. The C ring terminates in a 50-km-wide ringlet ($\tau_n \sim 0.4$) followed by a sharp transition to large optical depth ($\tau_n \sim 1$) within 6 km. This transition to the B ring is located at a radius of 92,066 km.

The detailed analysis of the UVS exit occultation data beyond the inner part of the B ring is not yet complete; however, several facts are apparent. In contrast to the C ring, the B ring can be characterized as having extensive regions of large optical depth interspersed with narrow regions of low optical depth or gaps. In about 40 percent of the B ring, between 1.72 and 1.89 R_S, no stellar signal was observed, indicating an average normal optical depth greater than 3.5. A preliminary look at the data in this region reveals no evidence of holes or gaps in the .1- to 3-km range having significant transmittance. The outermost portion of the A ring has a normal optical depth of $\tau_n \sim 0.6$. This region abruptly terminates in a few highly absorbed spectra indicating a ringlet with $\tau_n > 1$ and less than 3 to 6 km in width. This ringlet is located at a radius of 136,786 km.

Ring albedo. The UVS observed an extremely low level (<<1 *R* per angstrom) of reflected sunlight from the ring particles. This spectrum of the rings is nearly identical with a direct UVS spectrum of the sun as viewed through the occultation port. We have used the absolute solar spectrum of Donnelly and Pope (*16*) to estimate the absolute albedo of the rings at several wavelengths. In doing this we have assumed that the portion of the rings which fills our field (principally the B ring) is optically thick

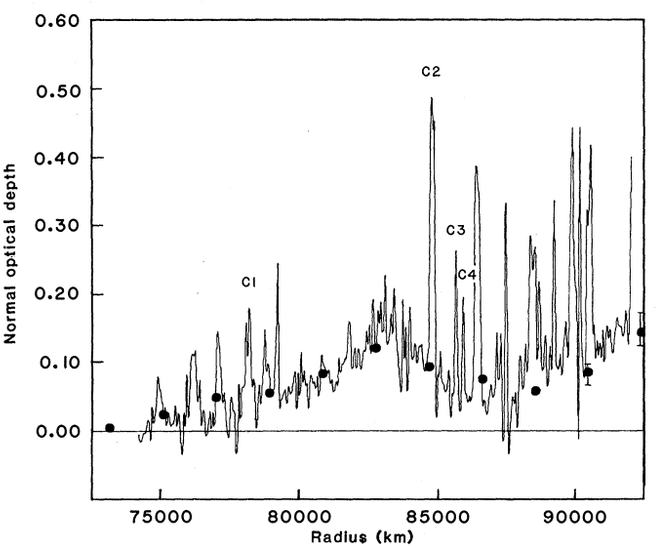

Fig. 4. Normal optical depths in the C ring determined by the UVS during the δ Sco exit of the rings. The Pioneer 11 (*15*) results (solid circles) have been plotted on the same scale for comparison. Peak values of optical depth in many of the narrow ringlets are diminished by the 50-km averaging used here. Ringlets labeled *C1*, *C2*, *C3*, and *C4* are shown at higher resolution in Fig. 5.

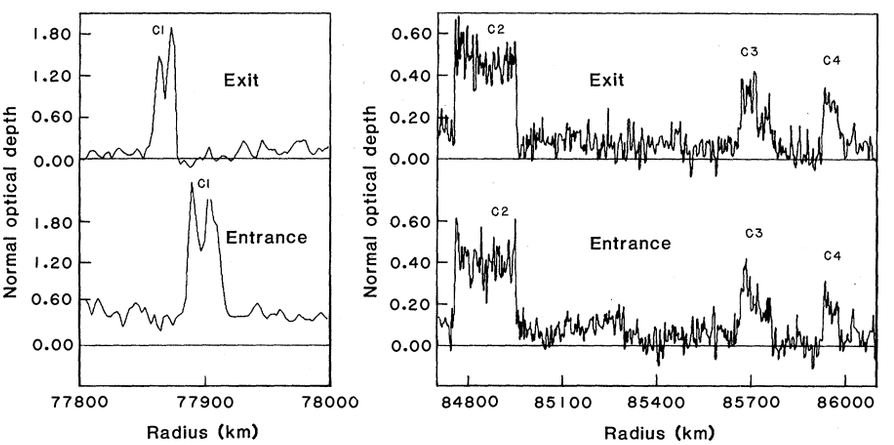

Fig. 5. A bilateral comparison of optical depths for two regions in the C ring observed by the UVS during entry and exit ring occultations. On the left, the section of the C ring containing an eccentric ringlet (*C1*). During exit this ringlet was both narrower and 32 km closer to the planet than during entrance. The appearance of larger optical depths for the entrance is caused by absorption in the atmosphere of Saturn. On the right, the portion of the C ring containing ringlets *C2*, *C3*, and *C4* is shown (see Fig. 4). The resolution is 3.3 km for the exit and 3.6 for the entrance.

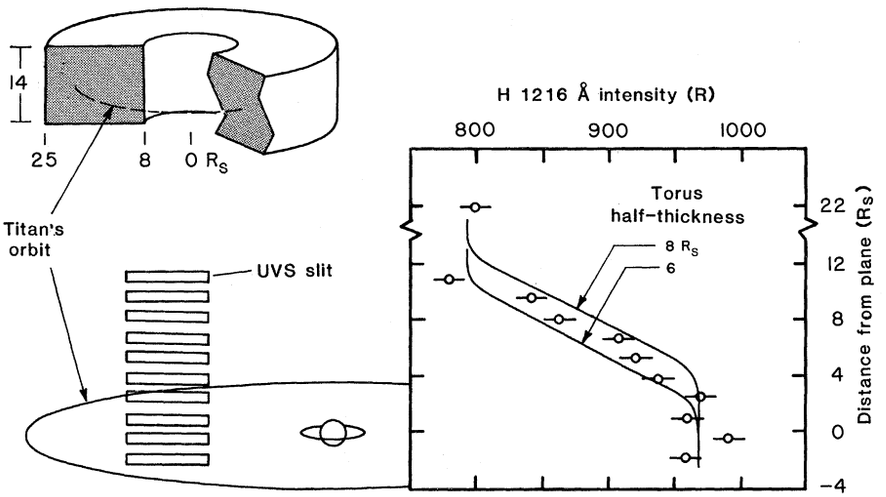

Fig. 6. The neutral hydrogen torus. Scanning as shown with the UVS slit oriented parallel to the orbital plane measured the H Lyα intensity distribution shown by the data points. The brightness variation expected for a cloud of uniform density, extending between 8 and 25 R_S in the orbital plane, is shown by the solid curves. The H distribution is the simple schematic form used in this preliminary model and does not represent the details of the expected density distribution.

and that the rings act as a Lambert surface in reflecting far-ultraviolet photons. These assumptions yield absolute albedos of 3.5 percent at 900 Å and 5 percent at 1304 and 1410 Å. These represent lower limits because of the assumption of optically thick rings. Laboratory measurements between 1200 and 1375 Å show that the reflectance spectrum of water ice is relatively flat (*17*) with an absolute albedo of ~ 5 percent to within a factor of 2. We are aware of no published measurements of the reflectance of water ice below 1200 Å. However, our comparison with the direct Voyager solar spectrum indicates a relatively flat reflectance spectrum between 1100 and 600 Å. One puzzling aspect of this observation was our failure to observe a similar albedo spectrum during the Voyager 1 encounter. Our viewing geometries were similar; however, the elevation of the sun with respect to the ring plane was 3.6° at the time of Voyager 1 whereas it was 8° for Voyager 2. This may indicate a strong dependence on solar elevation angle.

The presence of solar albedo from the sunlit side of the rings effectively limits the detectability of any emission from the vicinity of the rings which might be associated with the electrical discharges noted by the planetary radio astronomy experiment (*18*). We have used several hours of postencounter integration time obtained on the underside of the B ring, in the shadow of the planet, to search for such emission. Except for the case of the O I 1304 Å line our upper limits for neutral and ionized O are now a factor of 2 lower than those reported from Voyager 1 (*1*). For H I Lyman β our upper limit is 0.7 *R*.

Titan. The Voyager 2 observations of Titan were limited by distance from the planet and were compromised by the presence of a star in the field during the first long drift observation. The data were therefore of lower quality than those of the Voyager 1 Titan observations. However, the Voyager 1 Titan observations in the EUV first reported (*1*) have been analyzed in some detail (*19, 20*). The upper atmosphere is predominantly N_2 with an 8 percent CH_4 mixing ratio at a radial distance of 3700 km and 1 to 2 percent C_2H_2 at 3400 km. The exobase is at 3840 km where $[N_2] = 2.7 \times 10^8$ cm^{-3}, and $T = 186$ K. The sunlit face of the planet emits EUV radiation mostly from electron-excited N_2 (*19*). Upper limits have been placed on Ne I, Ar I, CO, H_2, and H I mixing ratios of 0.01, 0.06, 0.05, 0.06, and 0.1 respectively, at 3900 km, on the basis of the Voyager 1 EUV emission observations (*19*). The production of electron-excited emission appears to occur significantly only on the dayside face; detectable darkside emission is limited to H Lyα scattered radiation. The inferred electron energy dissipation rate was ~ 2×10^{10} W. This rather high deposition rate is difficult to explain in terms of energy available in magnetospheric electrons or in photoelectrons.

An important consideration for particle precipitation on Titan is the position of the solar wind bow shock. Near the time of Voyager 1 encounter, Titan was always inside Saturn's magnetosphere, whereas during the Voyager 2 encounter it was in the magnetosheath for substantial periods of time (*21*). In particular, Titan was in this position during the UVS observations at the minimum encounter distance [0630 SCET (spacecraft event time) 25 August]. The observed surface brightness in N_2 C_4'–X Rydberg band emission is very nearly the same as that observed by the Voyager 1 instrument. However, the Voyager 2 observation was on the downstream side of the sunlit hemisphere and this region would be expected to be less bright on the basis of Voyager 1 observations of the surface brightness distribution. This is consistent with earlier Voyager 2 observations at 1618 and 2045 SCET 25 August which show a factor of 2 greater brightness. During the period 24 and 25 August there is no evidence for strong intensity variation in the N_2 emissions, although the level of brightness is twice as high as the Voyager 1 encounter. There is no particular evidence relating the emission characteristics to the position of the bow shock relative to Titan's orbit either in intensity or spectral content.

The hydrogen torus. A cloud of neutral hydrogen atoms surrounding Saturn between 8 and 25 R_S was detected by the Voyager 1 UVS (*1*). This cloud is made up of H atoms that are formed in the atmosphere of Titan and escape from the satellite but are bound by the gravitational attraction of Saturn (*22*). Although the extent of the H torus in the equatorial plane was well determined, the extent perpendicular to this plane could not be well determined from the Voyager 1 data; consequently, the Voyager 2 observing sequence shown in Fig. 6 was designed. The variation of H Lyα intensity shown by the data points may be compared with the model calculations, which treat the vertical extent of the torus as the variable parameter. A half-thickness of 7 or 8 R_S matches the data quite well, in good agreement with the earlier upper limit of 6 R_S (*1*). The peak torus brightness of ~ 170 R is higher than the 100 R reported earlier, but this may be an effect of the convolution of the observing geometry with the H distribution above and below the oribtal plane, an effect not included in the model. A model path length of 44 R_S, a *g* value (*23*) of 2.4×10^{-3} sec^{-1} at 1 AU, and the assumption of an optically thin scattering medium imply an H density of ~ 20 cm^{-3}.

If the H atoms of the torus follow ballistic trajectories, the vertical extent of the torus implies that H atoms retain velocities of up to 1.9 km sec^{-1} after escaping Titan's gravity. For an exospheric temperature of 186 K (*20*), about

14 percent of the thermal H will have the necessary velocity of 2.9 km sec^{-1}, and chemical reactions can produce additional energetic H atoms (*19*). Hydrogen atoms leaving Titan with a velocity of 1.9 km sec^{-1} directed backward and forward along Titan's orbit would enter orbits taking them as close as 5.6 R_S and as far as 180 R_S from Saturn. The observed confinement of the H between 8 and 25 R_S can probably be explained by the fact that the lifetime of neutral hydrogen against ionization is $\sim 10^8$ sec between 10 and 21 R_S but falls rapidly by a factor of 100 inside and outside this region (*21*).

This lifetime is a factor of 10 longer than earlier estimates (*1*). If we use the new lifetime, and include the new estimates of the H density and the size of the torus reported here, the H supply rate from Titan is reduced by a factor of 2 to 1×10^{27} atoms per second. Titan model atmosphere calculations (*24, 25*) yield escape rates of this magnitude for both H and H_2, although Allen *et al.* (*26*) have obtained Titan loss rates for H and H_2 an order of magnitude higher. The long H lifetime means that collisions may be important in the torus. For a density of 20 cm^{-3}, the mean time between collisions is $\sim 10^8$ seconds, about the same as the H lifetime. It is possible that the H_2 density in the torus exceeds the H density (*1*), so that collisions would dominate the H distribution and treatment of individual particle orbits would not be useful. The appropriate formulation for a collision-dominated cloud (*24*) shows that its characteristic scale (to the 1/*e* density level) would be 8 R_S for a cloud temperature of 260 K.

B. R. SANDEL, D. E. SHEMANSKY
A. L. BROADFOOT, J. B. HOLBERG
G. R. SMITH
Earth and Space Sciences Institute, University of Southern California, Tucson, Arizona 85713
J. C. MCCONNELL
York University, Ontario, Canada M3J 1V3
D. F. STROBEL
Naval Research Laboratory, Washington, D.C. 20375
S. K. ATREYA, T. M. DONAHUE
University of Michigan, Ann Arbor 48109
H. W. MOOS
Johns Hopkins University, Baltimore, Maryland 21218
D. M. HUNTEN
University of Arizona, Tucson 85721
R. B. POMPHREY, S. LINICK
Jet Propulsion Laboratory, Pasadena, California 91103

References and Notes

1. A. L. Broadfoot *et al.*, *Science* **212**, 206 (1981).
2. The planet's brightness at He 584 Å is proportional to the flux in the solar 584-Å line, and the He 584-Å solar flux inferred from its correlation with the solar 10.7-cm flux is about the same at the two encounters. This implies a change in the atmosphere.
3. J. C. McConnell, B. R. Sandel, A. L. Broadfoot, *Planet. Space Sci.* **29**, 283 (1981).
4. The eddy diffusion coefficient K describes the effectiveness of vertical mixing of the atmosphere.
5. L. Wallace and D. M. Hunten, *Astrophys. J.* **182**, 1013 (1973).
6. Y. L. Yung and D. F. Strobel, *ibid.* **239**, 395 (1980).
7. J. C. McConnell *et al.*, in preparation.
8. A. L. Broadfoot *et al.*, *J. Geophys. Res.* **86**, 8259 (1981).
9. D. E. Shemansky *et al.*, in preparation.
10. J. M. Ajello, S. K. Srivastava, Y. L. Yung, G. R. Gladstone, in preparation.
11. D. E. Gerhart, *J. Chem. Phys.* **62**, 821 (1975).
12. B. R. Sandel and A. L. Broadfoot, *Nature (London)* **292**, 679 (1981).
13. M. L. Kaiser, M. D. Desch, A. Lecacheux, *ibid.*, p. 731.
14. L. W. Esposito, J. P. Dilley, J. W. Fountain, *J. Geophys. Res.* **85**, 5948 (1980).
15. The absolute planetocentric ring radii quoted in this report are based on event times and a preliminary Voyager 2 trajectory from the Jet Propulsion Laboratory. At present the largest uncertainty in the absolute radii of features is due to uncertainty in the location of Saturn's north rotation pole. We have used a pole located at 1950.0 right ascension of 38.554° and a declination of 83.316°. Current uncertainties in these values allow for an error of up to 30 km in the location of features in the ring plane.
16. R. F. Donnelly and J. H. Pope, *NOAA (Natl. Oceanic Atmos. Adm.) Tech. Rep. ERL 276-SEL 25* (1973).
17. B. Hapke, E. Wells, J. Wagner, W. Partlow, *Icarus*, in press.
18. J. W. Warwick *et al.*, *Science* **212**, 239 (1981).
19. D. F. Strobel and D. E. Shemansky, *J. Geophys. Res.*, in press.
20. G. R. Smith, D. F. Strobel, A. L. Broadfoot, B. R. Sandel, D. E. Shemansky, J. B. Holberg, *J. Geophys. Res.*, in press.
21. H. S. Bridge *et al.*, *Science* **215**, 563 (1982).
22. T. R. McDonough and N. M. Brice, *Icarus* **20**, 136 (1973).
23. A g value is defined as the scattering rate of photons in a solar line from a single atom. This rate varies inversely with the square of solar distance.
24. D. M. Hunten, in *Planetary Satellites*, J. A. Burns, Ed. (Univ. of Arizona Press, Tucson, 1977), p. 420.
25. D. F. Strobel, *Icarus* **21**, 466 (1974).
26. M. Allen, J. P. Pinto, Y. L. Yung, *Astrophys. J.* **242**, L125 (1980).
27. We thank the Voyager Project personnel at JPL for the enthusiastic efforts that have made this mission a success. We also thank the staff of the Earth and Space Sciences Institute, Tucson, for their untiring support. This work was supported by the Jet Propulsion Laboratory, California Institute of Technology, under NASA contract NAS 7-100. Additional support was provided by the Planetary Sciences Discipline of NASA's Office of Space Sciences.

10 November 1981

Radio Science with Voyager 2 at Saturn: Atmosphere and Ionosphere and the Masses of Mimas, Tethys, and Iapetus

Abstract. *Voyager 2 radio occultation measurements of Saturn's atmosphere probed to the 1.2-bar pressure level, where the temperature was 143 ± 6 K and the lapse rate apparently equaled the dry adiabatic value of 0.85 K per kilometer. The tropopause at both mid-latitude occultation locations (36.5°N and 31°S) was at a pressure level of about 70 millibars and a temperature of approximately 82 K. The stratospheric structures were very similar with the temperature rising to about 140 K at the 1-millibar pressure level. The peak electron concentrations sensed were 1.7×10^4 and 0.64×10^4 per cubic centimeter in the predawn (31°S) and late afternoon (36.5°N) locations. The topside plasma scale heights were about 1000 kilometers for the late afternoon profile, and 260 kilometers for the lower portions and 1100 kilometers for the upper portions of the topside predawn ionosphere. Radio measurements of the masses of Tethys and Iapetus yield $(7.55 \pm 0.90) \times 10^{20}$ and $(18.8 \pm 1.2) \times 10^{20}$ kilograms respectively; the Tethys-Mimas resonance theory then provides a derived mass for Mimas of $(0.455 \pm 0.054) \times 10^{20}$ kilograms. These values for Tethys and Mimas represent major increases from previously accepted ground-based values, and appear to reverse a suggested trend of increasing satellite density with orbital radius in the Saturnian system. Current results suggest the opposite trend, in which the intermediate-sized satellites of Saturn may represent several classes of objects that differ with respect to the relative amounts of water, ammonia, and methane ices incorporated at different temperatures during formation. The anomalously low density of Iapetus might then be explained as resulting from a large hydrocarbon content, and its unusually dark surface markings as another manifestation of this same material.*

Radio science observations at Saturn with Voyager 2 included (i) mid-latitude occultation studies in the northern and southern hemispheres, (ii) new, direct determinations of the masses of Tethys and Iapetus from radio tracking and an indirect determination of the mass of Mimas, and (iii) measurement of the near forward microwave scattering from ring C. Here we present results for the atmosphere and ionosphere of Saturn and the masses of Mimas, Tethys, and Iapetus (*1, 2*), plus a discussion of the mean densities of the satellites. The emphasis on various topics in this report reflects only the current state of our work. Other important questions, such as the structure of the lower ionosphere and the figure of Saturn, must await complete reduction of the data and the

0036-8075/82/0129-0553$01.00/0